Patterning of Epitaxial Perovskites from Micro and Nano Molded Stencil Masks

*Maarten Nijland, Antony George, Sean Thomas, Evert P. Houwman, Jing Xia, Dave H. A. Blank, Guus Rijnders, Gertjan Koster, and Johan E. ten Elshof**

A process is developed that combines soft lithographic molding with pulsed laser deposition (PLD) to make heteroepitaxial patterns of functional perovskite oxide materials. Micro- and nanostructures of sacrificial ZnO are made by micro molding in capillaries (MiMiC) and nano transfer molding, respectively, and used to screen the single crystalline substrates during subsequent PLD. ZnO is used because of its compatibility with the high temperatures reached during PLD and because of the ease of its removal after use by benefiting from its amphoteric nature. Sub-micrometer sized lines of $La_{0.67}Sr_{0.33}MnO_3$ are made by the transfer molding approach, preserving the anisotropic features expected for a fully oriented thin film and taking account for the magnetostatic contribution from the line shapes. Different patterns of $SrRuO_3$ are made with lateral dimensions of a few micrometers having individual features for which electrical isolation is illustrated. The bottom-up soft lithographic methods can be compliantly utilized for making epitaxial structures of various shapes and sizes in the μm down to the nm range, and offer unique opportunities for fundamental studies as well as for realizing technological applications.

1. Introduction

Physical vapor deposition techniques like pulsed laser deposition (PLD) have evolved to a level in which atomic scale control is achieved in the direction of film growth. The high degree of control has facilitated preparation of artificial oxide materials with properties that strongly diverge from those of the individual building blocks, and has made the exploration of a wealth of interesting phenomena possible.[1] The ability to control the lateral position of materials on substrates is also required to allow future device integration. Patterning of oxide films can be accomplished via collisions with highly energetic particles that selectively remove the undesired parts. An example is focused ion beam (FIB) milling, which is well developed and allows fabrication of sub-100 nm features,[2] but is limited by inherent drawbacks including deterioration of the generated surfaces and issues related to the serial nature of such top-down approaches.[3] When it comes to patterning of complete films on the scale of substrates or wafers, parallel patterning methods are required to overcome the time-consuming character and low throughputs that are inextricably bound to serial techniques.

Only a handful of methods are currently available that allow parallel patterning of thin films while keeping the crystallographic orientation in control. All of these techniques rely on the use of top-down fabricated stencil masks to shield parts of the substrate and enable bottom-up formation of epitaxial structures during their depositions. Efforts were made to apply reusable silicon nitride membranes during PLD,[4] but issues like the need to deviate from optimal deposition conditions, limitations in shapes, and rapid degradation of the masks, led to the development of sacrificial stencil masks. Particular interest has been given to anodic aluminum oxide (AAO) membranes, with which nm-sized epitaxial arrays of oxide nanodots were made, but owing to the self-organized formation of these membranes, patterns were poorly ordered and limited to a single shape of restricted sizes.[5] Photolithography was recently used to pattern sacrificial metal oxide stencil masks and fabricate epitaxial microstructures in arbitrary shapes, however, with lateral dimensions of several micrometers and with limited throughputs due to the vapor deposition step used to deposit the sacrificial metal oxide.[6]

In spite of all progress made in parallel patterning of metal oxide thin films, a facile method with which epitaxial micro- and nanostructures can be made in arbitrary shapes and with high fidelity is still lacking. Originally introduced by the group of Whitesides,[7,8] a family of bottom-up methods that uses patterned elastomeric masks, stamps, or molds, known collectively as 'soft lithography', has evolved to one of the most common approaches to pattern a wide range of different materials on micro- and nanometer length scales.[9] Inspired by the multitude of examples of structures made by soft lithography, we explored the potential of combining this technology with PLD, and show that we can profit from the distinct advantages of soft lithography while maintaining good control over nucleation and growth of technologically relevant perovskite oxides. Our

M. Nijland, Dr. A. George, Dr. E. P. Houwman, Prof. D. H. A. Blank, Prof. G. Rijnders, Dr. G. Koster, Prof. J. E. ten Elshof
MESA+ Institute for Nanotechnology
University of Twente
P.O. Box 217, 7500, AE, Enschede, The Netherlands
E-mail: j.e.tenelshof@utwente.nl
S. Thomas, Dr. J. Xia
Department of Physics and Astronomy
University of California
4129 Frederick Reines Hall, Irvine, CA 92697–4575, USA

DOI: 10.1002/adfm.201401170

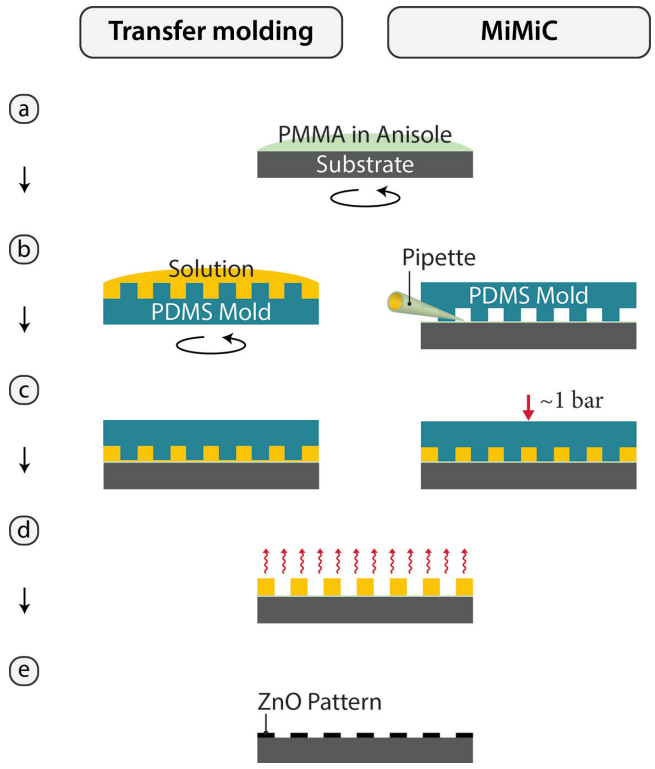

Figure 1. Schematic representations of the transfer molding and MiMiC processes to make ZnO stencil masks on single crystalline substrates for patterning of epitaxial oxides by PLD. In a first step, a) the substrate is coated with a thin layer of PMMA. In the case of transfer molding, b) the solution is spin coated on the mold, c) the mold is then placed on the substrate coated with the PMMA film, and the assembly is transferred to a hot stage at 80 °C to allow the pattern to cure. In the case of MiMiC, b) a PDMS mold is placed on the coated substrate and the precursor solution is added in front of the channels that are filled spontaneously by capillary action. After complete filling of the channels, c) the sample is heated to 60 °C and a pressure of ≈1 bar is applied to allow further curing. After curing the pattern (either made by MiMiC or transfer molding), d) the mold is removed and e) the sample is thermally annealed to convert the polymeric precursor into ZnO.

approach consists of two bottom-up fabrication steps: the first step is the molding of the sacrificial metal oxide stencil masks on single crystalline substrates (**Figure 1**), followed by the second step of PLD to form negative and fully-oriented replicas of perovskite-type oxide materials.

We used two types of soft lithography, namely micro molding in capillaries (MiMiC) and nano transfer molding. The transfer molding route was developed to fabricate stencil masks containing features with lateral sizes well below 1 µm, while MiMiC was employed to generate larger features. Comparing these two molding approaches, transfer molding requires optimized spin coating parameters to guarantee formation of structures that are sufficiently high but free from residues, while MiMiC does not require such optimization. MiMiC, on the other hand, is limited to open channels with dimensions in the micrometer range,[8] while no such fundamental limits apply to transfer molding. For this reason, both MiMiC and nano transfer molding were considered for the preparation of stencil masks with micrometer and nanometer dimensions, respectively. The stencil masks were made from ZnO, that was selected because of its excellent thermal stability and amphoterism. The first property is required to prevent any form of decomposition during high temperature PLD, and the latter property allows removal of these masks after use in either (weakly) acidic or basic environments, thus creating opportunities to use solutions in wide pH ranges in order to prevent degradation of the PLD grown epitaxial structures. Epitaxial patterns of $La_{0.67}Sr_{0.33}MnO_3$ and $SrRuO_3$ were formed at 750 °C and 700 °C, respectively, of which the crystallographic structure and properties closely resembled those of unpatterned thin films while additional functionality was added from the patterns. Both perovskite oxide materials were selected because of their potential use as electrode in all oxide epitaxial heterostructures,[10] for example, for ferroelectric capacitors,[11] micro-electromechanical systems (MEMS),[12] and field- effect transistors.[13] The half-metallic character[14,15] and high Curie temperature[16] of $La_{0.67}Sr_{0.33}MnO_3$, extend the possible field of application of this material into spintronic devices such as magnetic tunnel junctions.[15,17]

Summarizing, in the work presented here, we demonstrate that the combination of two powerful techniques, soft lithographic molding and PLD, leads to an unprecedented control of shape and crystallographic orientation. Soft lithographic molding is currently the only parallel patterning approach with which stencil masks can be made in arbitrary shapes, and sizes down to nanometer length scales. In addition, the methods presented here are fast, inexpensive, and practicable in any lab, as no dedicated equipment, nor clean room conditions are required. When used during PLD, the polycrystalline masks allow patterning of epitaxial oxides of which the crystallographic orientations are fully dictated by the underlying substrates. Keeping in mind the unrivaled properties found in epitaxial thin films and the challenges associated with patterning such materials, the approach presented in this work may be broadly utilized for future fundamental studies as well as for realizing (all oxide) devices.

2. Results and Discussion

2.1. Epitaxial Lines of $La_{0.67}Sr_{0.33}MnO_3$ Obtained with Nano Transfer Molded Stencil Masks

The nano transfer molding process to create stencil masks of ZnO is schematically illustrated in Figure 1 and is explained in more detail in the experimental section. In brief, complexes of Zn^{2+} with poly(acrylic acid) (PAA) were spin-cast on top of a polydimethylsiloxane (PDMS) mold, then transferred onto a substrate that was pre-coated with a thin layer of poly(methyl methacrylate) (PMMA), and decomposed into ZnO during subsequent thermal annealing. Numerous patterns were made on both Si and $SrTiO_3$, all with high fidelity and reproducibility. **Figure 2** shows one of the samples at different stages in the patterning process.

After molding, the samples were analyzed by optical microscopy and by observation of the interference colors from reflected light (Figure 2a). Generally, nearly the entire sample

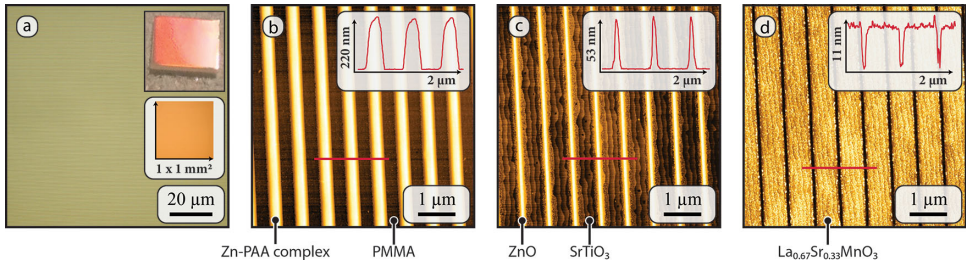

Figure 2. a) Optical microscopy image made directly after transfer molding, together with a photograph of the entire sample (upper inset) and microscopy image made at lower magnification (lower inset). b–d) Tapping-mode AFM height image of the same sample during subsequent steps in the patterning process, where the scanning direction was aligned to the principal crystal axis of the substrate. The AFM images were obtained b) before and c) after thermal treatment of the patterned complex of PAA and Zn^{2+} (in both cases after cleaning). Image (d) was obtained after PLD of $La_{0.67}Sr_{0.33}MnO_3$ and removal of the ZnO mask. The insets in (b–d) show height profiles as measured along the lines in the corresponding AFM images.

was covered with the pattern, even though the experiments were performed without specialized equipment in a lab without conditioning of environmental pollutants or humidity. The as-deposited organometallic lines were typically around 200 nm high, as is shown by the AFM height image in Figure 2b. During annealing the polymer degraded and ZnO formed, leading to significant shrinkage of the patterns in both vertical and horizontal directions. After annealing, the atomic steps on the substrates were well visible in between the lines of ZnO, indicating the absence of a residual layer in these regions. The lines of ZnO had relatively broad bases and to reduce the width of these bases, a pre-etching step was introduced in which the samples were exposed to a highly diluted solution of hydrochloric acid, leaving a pattern of ZnO as shown in Figure 2c. These patterns were used as stencil masks during subsequent high-temperature depositions of $La_{0.67}Sr_{0.33}MnO_3$. Reflection high energy electron diffraction (RHEED) was used during these depositions to control the final layer thickness to 10.0 nm (supporting information). Figure 2d shows isolated lines of $La_{0.67}Sr_{0.33}MnO_3$ (having a width of 620 nm and a spacing of 80 nm) that were obtained after PLD and etching of the ZnO mask.

All substrates were covered with a thin layer of PMMA before patterning, so that the process could be optimized independent of the underlying substrate. This step led to a more universal process that could be carried out on arbitrary substrates, and allowed us to optimize patterning on Si substrates, after which we could repeat the procedure on $SrTiO_3$. The polymeric films were removed during thermal annealing, and results discussed below showed no indications for an influence of this way of removal on subsequent growth of epitaxial films. The presence of trace amounts of organic contaminations can not be excluded though, but may be avoided either by dissolving the polymer directly after molding or by not using the coating at all. Regarding the first option, PMMA can be dissolved in a solvent like acetone (without affecting the organometallic patterns), followed by submerging the samples in ethanol and drying in N_2. Note that this sequence is also used after single termination treatments,[18] and may thus be useful when the uncovered parts of substrates should be perfectly free from organic residues. Patterning was also possible when the use of a coating was omitted, but led to a reduced reproducibility of the molding step on $SrTiO_3$.

The organometallic lines obtained after patterning were uniform in dimensions and shape, but they were generally not perfectly symmetrical as can be seen from the profile in the inset of Figure 2b. The observed slight asymmetry may be due to cohesive rupturing of the organometallic lines during removal of the mold, as discussed further on in this section. The samples were annealed by rapid thermal annealing, and resulting decomposition and densification led to significant shrinkage, about a factor of four in height and more than a factor of three in width. Also the shape of the patterns changed during thermal treatment, leading to narrow lines (FWHM $\approx$ 85 nm) that widened near their valleys, indicating that motion of material at the bottom of the lines was impeded by clamping with the substrates. To obtain a more square-shaped form, samples were shortly immersed in a weakly acidic solution of hydrochloric acid (pH = 4.1), during which the width at the bottom of the lines reduced significantly while the FWHM was barely affected. We note that shrinkage may be controlled by various means, for instance by changing the concentration or contents of the solution, or by using a different mold design.

When the precursor solution was added to the PDMS mold, its channels filled and the concentration of Zn^{2+} increased as a consequence of solvent evaporation and diffusion into the mold. Using the area A of a single channel of arbitrary length l, the initial number of zinc cations in volume Al can be calculated from the concentration of the parent solution. Provided that only fully densified ZnO was left after thermal treatment, the final number of zinc cations in a typical patterned line of length l was determined by integrating the AFM height profile as displayed in the inset of Figure 2c. Comparing the two values, almost 15 times the amount of Zn was present in the annealed structures than directly after infiltrating the mold. These calculations strongly indicate that filling of the channels by solution from the outside continued even at an advanced stage of drying, a process that is essential for obtaining structures that are sufficiently high to be used as stencil masks.

Patterns could be made without residual layers between the patterned ZnO features, even though no pressure was applied on the mold during curing and also when the washing step before annealing was skipped (this conclusion was made from the visibility of atomic steps after the annealing process). In contrast, we note that soft lithographic patterning is generally

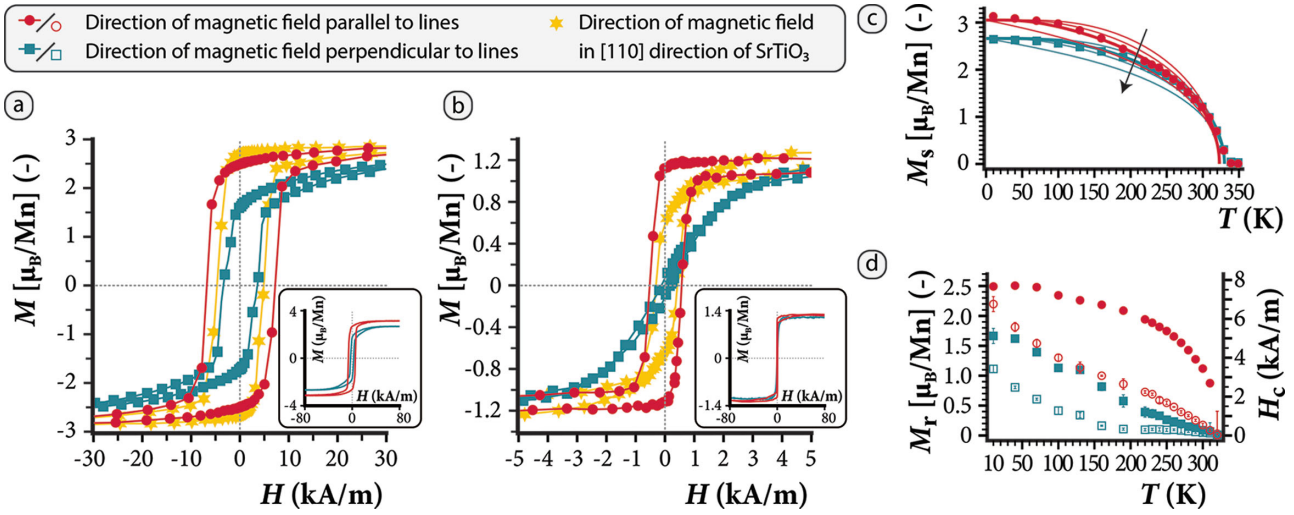

Figure 3. Magnetic characterization of the line pattern of Figure 2d measured by VSM. Magnetic hysteresis curves are given at a) 10 K and b) 300 K, where the field was applied parallel ([100]), perpendicular ([010]) and at 45° ([110]) to the lines. The insets in these figures show the dependence of magnetization over a larger range of magnetic fields for the parallel and perpendicular case. The temperature dependence of saturation magnetization is plotted in (c), together with fits to a Brillouin functional dependency for different total angular momentum quantum numbers (J = 1, 2, 4, ∞ and increases in the direction of the arrow). In image (d), remnant magnetization (closed symbols) and coercive field (open symbols) are plotted versus temperature.

associated with residuals, either by transfer of oligomers from the mold[19] or by incomplete expulsion of the fluid.[20] In related work describing an edge printing process, absence of residual layers was observed and explained by a relative large adhesive strength between PDMS and PAA.[21] The complex of PAA and Zn^{2+} is expected to cover the entire sample during patterning, forming a thin layer that protects the sample from interactions with oligomers on the PDMS mold. When the mold is removed this protective layer is removed as well due to a larger adhesive strength with PDMS than with the PMMA film on the substrate. The precursor that is present in the grooves of the mold is more prone to cohesive failure, leading to successful transfer in these regions.

After deposition, the original atomic terraces on the surface of the substrate were replicated on the patterns of $La_{0.67}Sr_{0.33}MnO_3$ and the films were uniform up to the edges of the structures (Figure 2d). The root mean square (RMS) roughness of a typical line (0.32 nm) confirmed smooth growth and was only slightly higher than the roughness measured on an unpatterned film that was deposited under the same conditions (0.20 nm). Epitaxy was confirmed by electron backscatter diffraction (EBSD), which indicated a single orientation of the patterns even at their edges (supporting information). No detrimental effects of etching the stencil masks were found in the structures of $La_{0.67}Sr_{0.33}MnO_3$, as no significant changes in film topography (roughness) were observed before and after removal of the stencil masks, and characterization discussed below indicated ferromagnetic properties of a well-oriented film of $La_{0.67}Sr_{0.33}MnO_3$. The polycrystalline ZnO stencil masks disintegrates both under acidic and basic conditions, and for this work only highly diluted solutions of hydrochloric acid were used for etching. In the case of using a solution of pH = 4.1, etch rates were found already to be sufficiently fast, in the order of ≈0.5 nm s^{-1}.

2.2. High Quality Epitaxial Patterns Indicated by Magnetic Characterization

Merely considering growth dynamics and topography is not sufficient to conclude about the quality of a film (as defined by Boschker et al.[22], since properties also strongly depend on other factors like oxygen stoichiometry[23] and epitaxial strain.[24] For this reason the effect of patterning was further studied by comparing the ferromagnetic properties of lines of $La_{0.67}Sr_{0.33}MnO_3$ with those measured in a thin film deposited under the same conditions. Magnetic properties were measured primarily to study the influence of patterning on the quality of the epitaxial films, and to illustrate control over anisotropy resulting from the patterns. An external magnetic field was applied in the plane of the film in different directions and for each case magnetization was measured in the same direction as the external field. Magnetic hysteresis loops of the patterned sample at 10 K and 300 K are shown in **Figure 3**, and the temperature dependencies of saturation magnetization (M_s), remnant magnetization (M_r) and coercive field (H_c) are also displayed in this figure (similar characterization of the unpatterned thin film is included in the supporting information).

When the field was applied perpendicular to the lines, more slanted curves with lower coercive field and remnant magnetization were obtained as compared to the curves obtained with parallel magnetization. The patterns of $La_{0.67}Sr_{0.33}MnO_3$ had an absolute saturation magnetization of $M_{0,s}$ = 3.1 μ_B/Mn and a Curie temperature around T_C = 331 K. Note that the calculated value of magnetization per Mn is not as accurate as that for unpatterned films, since calculations are based on topographical information (Figure 2d) to determine the coverage of the lines of $La_{0.67}Sr_{0.33}MnO_3$ (alternatively, the coverage of the lines of ZnO can be determined from Figure 2c to estimate the amount of $La_{0.67}Sr_{0.33}MnO_3$, yielding $M_{0,s}$ = 3.5 μ_B/Mn).

For the patterns of $La_{0.67}Sr_{0.33}MnO_3$ various sources of magnetic anisotropy are expected, in particular magnetostatic anisotropy from the line shapes, magnetocrystalline anisotropy from crystal field interaction and spin orbit coupling, and anisotropy induced by the step edges.[25] The contributions from these sources to the total anisotropy can be found in the supporting information, where different routes are described to calculate the demagnetizing factor, theoretically from the geometry of the patterns and experimentally from fitting hysteresis curves. From our experiments we obtained a demagnetization factor of $N_\perp - N_\parallel = 0.015$, and conclude that the line patterns can be described by elliptic cylinders with thickness $a = 10$ nm, length $b = 5$ mm $\approx \infty$ (yielding $N_\parallel = 0$) and width $c = 600$ nm, as this approximation yields $N_\perp = 0.016$.[26] Note that the hysteresis curves were obtained from bulk measurements, meaning that the shapes of these curves reflect the uniformity of the patterns over the complete areas of the samples. The linearity of shearing that was observed in the case of magnetization perpendicular to the lines at 300 K, leads to the conclusion that transfer molded stencil masks allow fabrication of uniform patterns over areas of at least 5 mm × 5 mm.

Despite the clear effects of patterning on ferromagnetic hysteresis, magnetic characterization indicated only a minor influence of patterning on the quality of the films. That is, the absolute saturation magnetization and Curie temperature measured for the epitaxial lines strongly resembled those measured on an unpatterned film (for the thin film $M_{0,s} = 3.5\ \mu_B$/Mn and $T_C = 334$ K were obtained). These similarities confirm the ability to maintain a high degree of control during film growth while using stencil masks made by nano transfer molding.

2.3. Epitaxial Patterns of $SrRuO_3$ Obtained with Stencil Masks Made by MiMiC

To illustrate flexibility in terms of size ranges, shapes, and deposited material, soft lithographic molding was used to make stencil masks of various shapes for fabrication of epitaxial micropatterns of $SrRuO_3$. As noted in the introduction, micro molding in capillaries (MiMiC) was used, which is preferable to transfer molding because it requires fewer experimental parameters to be optimized. The process of making the stencil masks is essentially similar to the transfer molding process, except that the channels are filled by capillary action while the mold is attached to the substrate, as schematically shown in Figure 1. Note that alternatively, a photolithographic approach can be used to pattern stencil masks of arbitrary shapes with micrometer dimensions,[6] but MiMiC offers distinct advantages in that it requires less experimental operations and is far less time consuming than a photolithographic approach. **Figure 4** show results from fabricating and characterizing the microstructures of $SrRuO_3$ (having lateral dimensions around 4–7 μm, separated by 0.5–7 μm) that were patterned into lines (Figure 4a–d) and triangles (Figure 4e–h).

After MiMiC, both samples were completely covered with the desired patterns as was observed by optical microscopy and by

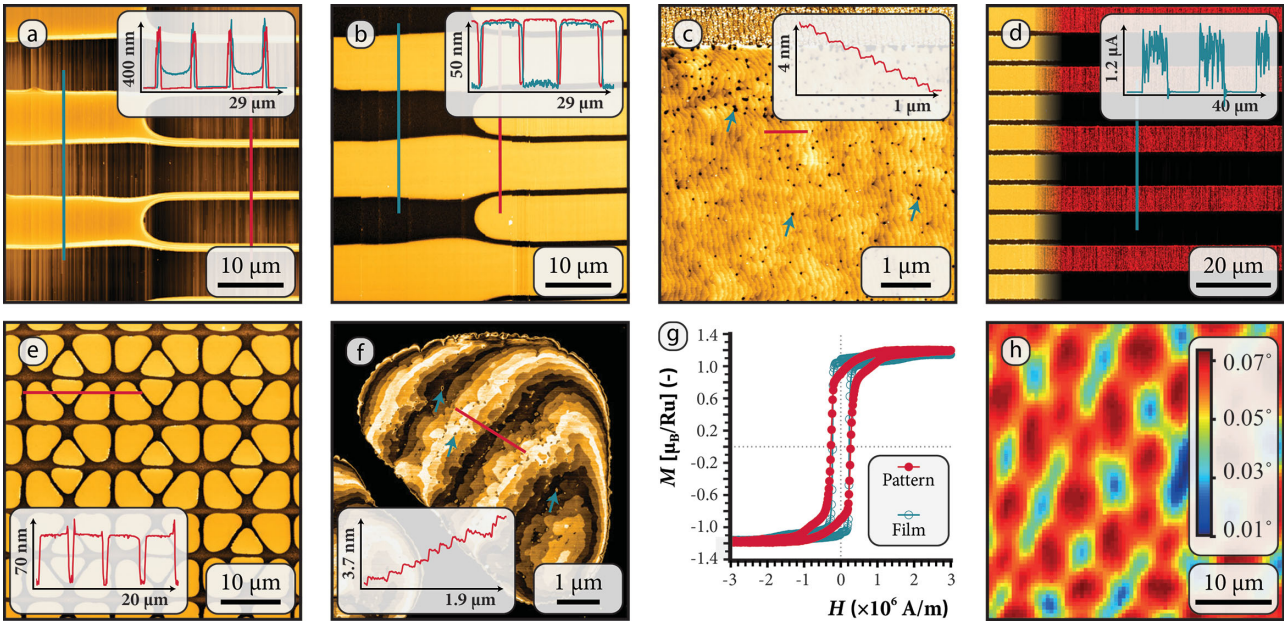

Figure 4. Fabrication and characterization of patterns of a–d) lines and e–h) triangles on $SrTiO_3$ made by MiMiC and followed by deposition of epitaxial $SrRuO_3$. Tapping mode AFM height images show a sample a) before and b,c) after PLD and subsequent dissolution of the ZnO mask. The tunneling AFM (TUNA) image in (d) was recorded with a sample bias of 1.5 V DC for which every two lines only one was connected to a back electrode (ground). On the left side of the image the corresponding height image is overlayed and the inset shows the current profile measured along the vertical line in the main image. Image (e,f) show AFM height images of a different pattern of $SrRuO_3$ after removal of the ZnO mask. Magnetic hysteresis loops of this sample and an unpatterned film of $SrRuO_3$ are plotted in (g); the VSM measurement was conducted at 10 K and the field was applied perpendicular to the surface of the sample. The map scan in image (h) shows the Kerr signal of the patterned sample as obtained by optical magnetometry at 78 K after cooling the sample in a field of 2 KG. The insets in image (a–c,e,f) are height profiles measured along the lines in the corresponding images.

eye looking at the color from interference of reflected light. The lines were designed such that at one side of the sample twice as many lines were present as compared to the opposite side of the sample. Figure 4a shows the ZnO mask at the transition region, where clear differences are seen between the shape of the narrow and broad lines. The broad lines were on average lower than the narrow lines and were clearly highest at the edges. This edge effect was previously observed and explained by preferential wetting and drying at the corners of the PDMS mold.[27] Although the height of the ZnO structures did depend on the exact shape of the mold, no significant variations were measured at different locations on the samples as long as the geometry was the same. Similarly as for the patterns made by transfer molding, we calculated that the narrow (broad) lines contained 17 (14) times more material than could be expected from complete filling of the channels with the original solution. Although the patterns will not have reached the bulk density of ZnO, the significant numbers prove that filling and drying occurred simultaneously.

For the line patterns, the deposition of $SrRuO_3$ was followed with RHEED (supporting information). The observed oscillations were typical for growth of $SrRuO_3$ on $SrTiO_3$ terminated on the TiO_2 plane,[28] as was concluded from a nearly doubled width of the first oscillation as compared to subsequent ones. A coherently grown pattern with in-plane lattice constants equal to that of the substrate was confirmed by reciprocal space mapping (supporting information), indicating that epitaxial strain was preserved after removal of the mask. Most clearly illustrated by the AFM image of Figure 4f, surface steps bended away from the direction of the steps of the substrate: a process that resulted from step flow growth in confined areas, as further explained in the supporting information. The patterns of $SrRuO_3$ were mostly atomically flat up to the edges, but contained pits that were mainly situated at the atomic step ledges. The pits were concentrated at the edges of the line pattern (Figure 4c), while for the triangles pits were predominantly observed near their centers (Figure 4f; in both images, three blue arrows are used to indicate three such pits). Growth of $SrRuO_3$ is highly sensitive to the chemistry of the underlying substrate, and for a purely TiO_2 terminated substrate, smooth films are expected to grow in a step flow growth mode.[28,29] Pits were observed even in a film made for reference, which was deposited under the same conditions on a $SrTiO_3$ substrate that was treated to obtain a single TiO_2 termination. The presence of pits even without patterning indicates that the pits were not solely the result of the patterning process, although the uneven distribution indicates that there was at least some effect from patterning.

The line patterns were characterized by tunneling AFM (TUNA), imaging height and tunneling current simultaneously. The tunneling current map is shown in Figure 4d and the corresponding height image is overlayed on the left side of the image. The special design of the line pattern was used to connect only half of the lines, which is why for every two lines only one showed conductivity. This result proves that the lines were electrically isolated from each other, though it should be noted that this was only the case after post-annealing (the result before post-annealing can be found in the supporting information). Possibly oxygen vacancies were formed near the surface of the substrate during formation of the ZnO stencil mask, rendering the surface of $SrTiO_3$ conductive. By post-annealing the sample in oxygen for 4 h at 600 °C after removal of the stencil mask, vacancies were filled and leakage was prevented.

In order to obtain a better understanding of the effects of the used patterning route on the quality of the heteroepitaxial features of $SrRuO_3$, magnetic characterization was performed on the triangular pattern and compared to the case of an unpatterned thin film. Measurements were performed by using a vibrating sample magnetometer (VSM) and a scanning optical magnetometer using the polar magneto-optic Kerr effect (MOKE).[30] The typical shape of the patterns is reflected by the magnetic map in Figure 4h, in which the gradual change of the Kerr signal was due to the probe size of the experimental method (≈2 μm). The Curie temperature of the sample was determined as $T_C \approx 150$ K, which (in line with the diffraction results) points to preservation of epitaxial strain inside the structures.[31] The hysteresis curve that resulted from VSM analysis is shown in Figure 4g and was obtained at 10 K with the field applied out of the surface plane. A hysteresis curve of the unpatterned film is shown as well, for which similar saturation magnetization and coercivity were measured. The most prominent difference between the two curves is the reduction of squareness that is observed for the patterned sample, indicating that extra energy was needed to rotate the magnetization vector out of the surface plane in the case of the patterned sample. The rounding is possibly the result of a local change of the magnetocrystalline anisotropy due to partial relaxation of the stress, either at the imperfections (as indicated by the higher number of pits in the AFM images) or near the edges of the patterns. Additional proof for partial stress relaxation was obtained from X-ray diffraction (supporting information), since broader and more asymmetric film peaks were observed for the patterns than for the unpatterned thin film. The minor differences between the ferromagnetic behavior of the two films, once again points to near complete preservation of control of thin film growth after using the MiMiC route.

3. Conclusions

Soft lithographic molding techniques were used to make stencil masks of ZnO directly on single crystalline substrates, with which isolated features of epitaxial perovskite oxides were obtained after pulsed laser deposition and lift-off. The bottom-up approach presented in this work is more than a supplement to currently available alternatives, as functional structures of $La_{0.67}Sr_{0.33}MnO_3$ and $SrRuO_3$ were made that can neither be fabricated by state-of-the-art shadow masking nor by using self-organized AAO membranes. Micro molding in capillaries (MiMiC) and transfer molding were used complementary to cover both the micrometer and nanometer lateral size range, for which we note that both methods allowed fabrication of residue-free patterns of ZnO with high fidelity over the entire area of the substrate. Both molding approaches did not compromise in the control over growth that is generally achieved for unpatterned films, as surface morphology, RHEED patterns, crystal structure and magnetic properties of patterned and unpatterned films were comparable. Besides, new functionality was added

as e.g. magnetic anisotropy of the lines of $La_{0.67}Sr_{0.33}MnO_3$ was mainly dictated by the patterns, and electrical isolation of the structures was demonstrated for the lines of $SrRuO_3$. Next to these effects acting on the entire structures, signatures of local effects were measured in both materials that may be the result of relaxation and ensuing strain gradients at the surfaces, offering unique opportunities to locally engineer strain in epitaxial thin films.

As a final note we would like to point out that ZnO structures made by transfer molding and MiMiC in itself may find uses other than as thermally stable sacrificial stencil mask. All ZnO structures presented in this work were well organized over the complete sample areas and were free from residues. ZnO is a wide bandgap semiconductor (with a bandgap of 3.37 eV) with an exciton binding energy (60 meV) significantly larger than the thermal energy at room temperature (26 meV). Interest in this material has mainly been focused on its optical properties, in particular its sharp emission in the near-UV wavelengths for laser applications.[32] The conductivity of ZnO is highly sensitive to dopants, adsorbates, interstitials and oxygen vacancies, making it an interesting candidate for transparent conducting and gas sensing applications.[33] At least some of the aforementioned applications may be realized with the methods presented in this work.

4. Experimental Methods

Chemicals and Materials: Zinc nitrate hexahydrate ($Zn(NO_3)_2{\cdot}6H_2O$, reagent grade, 98%) and poly(acrylic acid) (Mw ≈ 1800 g mol^{-1}) were purchased from Sigma-Aldrich. A commercial solution of 2% w/w poly(methyl methacrylate) (Mw ≈ 950 000 g mol^{-1}) in anisole was obtained from MicroChem. Anisole (99%) and ethanol (99.8%) were acquired from Merck and Assink Chemie, respectively. An ammonium fluoride etching mixture (AF 875–125, puranal) from Honeywell was used in a fume hood inside a lab with an emergency Hexafluorine washing station while wearing protective gloves, protective clothes and eye protection. Ultrapure water with a resistivity of 18.2 MΩ cm was used. All chemicals were used as received, without additional purification. Two different solutions were prepared: an aqueous one for the transfer molding process and one in ethanol for MiMiC. For the aqueous solution 0.18 g PAA was completely dissolved in 6 mL water and then 0.36 g $Zn(NO_3)_2{\cdot}6H_2O$ was added. The other solution was prepared by dissolving 0.36 g PAA in 5 mL ethanol and subsequent addition of 0.3 g $Zn(NO_3)_2{\cdot}6H_2O$. Both solutions were stirred for at least 48 h after which they were stored and used within three months. Nanopatterned silicon masters (part number SNS-C14.3–0808–350-D45-P) were purchased from LightSmyth Technologies (Eugene, United States) and micropatterned silicon wafers with a 1 μm oxide layer were obtained from LioniX B.V (Enschede, the Netherlands). The nanopatterned masters were left in the straw (as received) and placed vertically in a desiccator together with a beaker containing 2 μL 1H,1H,2H,2H-perfluorooctyltrichlorosilane (Fischer Scientific, 97%). The glass desiccator was then pumped down to 10 mbar with a chemistry pumping unit (PC 3001 Vario Pro, Vacuubrand), closed off, and left for 13 to 14 h. The micropatterned masters were silanized with a comparable procedure. A Sylgard 184 silicone elastomer kit from Dow Corning was used to prepare polydimethylsiloxane (PDMS). The base agent and curing agent were properly mixed in a 10 to 1 weight ratio by mechanical stirring. Air bubbles were subsequently removed in a glass desiccator that was pumped down for at least 10 min with a standard diaphragm vacuum pump (Vacuubrand). The desired silanized master was placed on a piece of weighing paper on a cold heating plate and was surrounded by a ring of Teflon. The PDMS was then poured on the silanized master and cured at 60 °C for at least 24 h. Single crystal (001) oriented $SrTiO_3$ substrates (5 mm × 5 mm) were purchased from CrysTec GmbH. These substrates were treated to obtain a single TiO_2 termination according to the procedure of Koster et al.[18] The substrates where then protected with a thin layer of PMMA by spin coating 30 μL of a 1% w/w solution of PMMA in anisole yielding a layer thickness of approximately 20 nm. The liquid was added to the spin coater (WS-400B- 6NPP, Laurell Technologies Corporation) during a spin on stage at 500 revolutions min^{-1}. After 5 s, the spinner accelerated to 6000 revolutions min^{-1} and decelerated 60 s later until it came to a halt. The acceleration or deceleration between every step was fixed at 27.5 revolutions s^{-2}. The substrate was subsequently transferred to a hot plate at 160 °C and covered with a Petri dish. After 2 min, the substrate coated with the ≈20 nm thick PMMA film was stored.

Nano Transfer Molding: Prior to transfer molding, the mold was released from the master and cut to 8 mm × 8 mm. Both mold and substrate were cleaned by oxygen plasma (Harrick plasma) at 30 W for 2 min. The thickness of the PMMA film on the $SrTiO_3$ substrate had reduced to ≈6 nm after this step. The mold was then placed on a flat puck that was placed inside the spin coater and held by vacuum. Prior to actual spin coating, the mold was exposed to a pulse of N_2 gas, 30 μL of the precursor solution was added to the mold, and complete wetting of the mold was confirmed. Spin coating was then initiated according to the program of **Table 1** where the acceleration was 27.5 revolutions s^{-2} between each step. After spin coating, the mold was observed by optical microscopy to confirm formation of a smooth film without significant contamination. Directly after this step the mold was placed onto the substrate and carefully pressed to ensure complete adhesion. The assembly was then transferred to a pre-heated hot stage at 80 °C and left there for 45 min to allow the pattern to cure. The mold was released from the substrate and proper transfer was confirmed by optical microscopy and AFM. Prior to annealing the patterns, the samples were cleaned by repeated dipping in a water bath for 10 s, followed by dipping in ethanol and drying in a stream of N_2. This step was introduced to rinse away all species that were not part of the (cross-linked) PAA-Zn complex. The adhesive strength between the patterns and the substrates was found to depend on the humidity of the environment during patterning, where a high humidity was favorable for stronger adhesion. The patterns were then annealed in a pre-heated microwave furnace (Microsynth, Milestone Srl) at 750 °C for 15 min.

Micro Molding in Capillaries: Just before patterning by micro molding in capillaries (MiMiC), the desired micropatterned mold was cut into sizes of 10 mm × 10 mm and cleaned by ultrasonication in ethanol for 5 min. The mold was then dried in a stream of N_2 and stored in a Petri dish. A microscope slide (Thermo Scientific) was cleaned on a hot plate at 250 °C with a jet of supercritical CO_2. Together with the substrate, the glass plate was subsequently cleaned by oxygen plasma at 30 W for 2 min. The mold was placed on the microscope slide, carefully pressed to ensure full adhesion and directly pulled off. The substrate was then placed on the other side of the microscope slide and the mold was placed on the substrate and carefully pressed. Using a pipette, 30 μL of the precursor solution was placed just in front of the mold, after which initial filling of the channels was confirmed by optical microscopy. MiMiC was continued in the middle of a closed Petri dish containing a few droplets of ethanol at the sides. After 60 min, the microscopy slide was transferred to a homemade molding machine and a pressure of ≈1 bar was applied on the mold and substrate to guarantee proper contact between the two. Maintaining the pressure, the sample was heated from room temperature to 60 °C, without allowing the temperature to overshoot. The assembly was released from the molding machine after 2 h, the mold was removed from the substrate and proper

Table 1. Program used for spin coating a solution on a mold during transfer molding.

t [s]	15	5	180	15
v [revolutions min^{-1}]	500	1000	5000	500

transfer of the pattern was confirmed by optical microscopy. The sample was then annealed in the microwave furnace under the conditions given in **Table 2**.

Pulsed Laser Deposition: Before PLD, the samples were cleaned by repeated dipping in a bath of 0.0004% w/w hydrochloric acid. Samples made by transfer molding were dipped into the solution for 5 s and samples made by MiMiC were cleaned for 30 s. Directly after this step, the samples were quickly immersed in a beaker containing water (to stop the slow dissolution of ZnO by the acid), then in a beaker containing ethanol and were then dried in a jet of N_2. $La_{0.67}Sr_{0.33}MnO_3$ was deposited on the samples patterned by transfer molding. Depositions were carried out in an O_2 environment of 0.27 mbar. The temperature of the samples during depositions was controlled by a thermocouple inside the heater that was set at 750 °C. The laser beam was produced by a 248 nm KrF excimer laser (LPXPro from Coherent, Inc.) with a typical pulse duration of 20 to 30 ns, operated at 21.5 kV. A square mask of 99 mm^2 was used to select the most homogeneous part of the laser beam. The laser was then focused on the stoichiometric $La_{0.67}Sr_{0.33}MnO_3$ target (Praxair electronics) with a spot size of 2.3 mm^2. Laser fluence was controlled with a variable attenuator at 2.0 J cm^{-2}. For all depositions, target and sample were directly facing each other at a distance of 5 cm. The target was pre-ablated at 5 Hz for 2 min to remove possible surface contaminations. Depositions were performed at 1 Hz and deposition times were varied to yield a layer thickness of 26 monolayers. Growth was monitored in situ by RHEED, allowing the determination of growth rate on a unit cell level and studying growth dynamics. After deposition, the PLD chamber was filled with O_2 to 100 mbar and the heater power was turned off to allow cooling to room temperature. $SrRuO_3$ was deposited on the samples patterned by MiMiC. Depositions were performed in an O_2 environment of 0.08 mbar at a heater temperature of 700 °C. An image of a square mask with rounded corners (56 mm^2) with a size of 1.8 mm^2 was produced on the stoichiometric $SrRuO_3$ target (Praxair electronics). A variable attenuator was used to adjust the laser fluence to 2.1 J cm^{-2} on the target. The target was pre-ablated at 5 Hz for 6 min and depositions were carried out at 2 Hz for 30 min (corresponding to a final layer thickness of ≈50 nm). After deposition, the samples were allowed to cool to room temperature at a maximum rate of 20 °C min^{-1} in an environment of 100 mbar O_2. The patterns of ZnO were removed by ultrasonication in an aqueous solution of 0.04% *w/w* hydrochloric acid for 5 min. Ultrasonication was repeated twice in water and once in ethanol, all for 2 min. The sample was then dipped in ethanol and dried on lens paper (LENSX 90 from Berkshire).

Analysis and Characterization: The topography of the samples was analyzed with a Dimension Icon atomic force microscope (Bruker AXS) using the standard tapping mode option. A selected sample was further studied using the tunneling AFM option. The data were processed using Gwyddion 2.30, and some images were additionally analyzed by ImageJ 1.46r. The height images from the samples made by transfer molding were visualized with the adaptive nonlinear color mapping option, whereas the samples made by MiMiC were visualized with a linear color range. ImageJ was used to determine the relative coverage of the patterns, which was used as input for calculation of the magnetic moment per cation. Crystallographic information was obtained with an X'Pert PRO MRD (PANalytical) using the parallel beam mirror, monochromator and PIXcel 3D detector modules. The polar and in-plane miscut angles of the substrates were determined from the ω-offsets of the (202) and (022) diffraction planes and corresponding optical planes (values for selected samples can be found in the supporting information). Further crystallographic information was obtained by EBSD performed on a Merlin field emission microscope (Zeiss) equipped with an angle selective backscatter detector. Magnetization measurements were conducted on a vibrating sample magnetometer (Physical Properties Measurement System by Quantum Design). The magnetic moments were determined as a function of the magnetic field and temperature, where the applied field and measured magnetization were along the same direction. Most samples were cut with a wafering blade (Isomet, Buehler) in order to fit into the pick-up coil for measurements in the out-of-plane and [110] directions. For selected samples, the temperature dependence of the saturation magnetization was determined and fitted to the Brillouin functions from Weiss theory of ferromagnetism assuming no external field and for different total angular momenta (J). Best fits were obtained by iteratively changing Curie temperature (T_C) and absolute saturation magnetization $M_{S,abs}$ and determining least squares. T_C and $M_{S,abs}$ were then chosen from the best fit. Shifts of the hysteresis loops in $H_{external}$ were corrected by measuring a Pd reference sample after every measurement at 300 K. Magnetization was also studied by a modified Sagnac interferometer, which could map the out-of-plane magnetization by making use of the polar magneto-optic Kerr effect (MOKE).[30] The error bars and deviations used in the article all represent a confidence of 95% (two times the standard deviation).

Table 2. Temperature program used to anneal the patterns made by MiMiC with a microwave furnace.

t [min]	15	15	9	30
T [°C]	400	400	620	620

Supporting Information

Supporting Information is available from the Wiley Online Library or from the author.

Acknowledgements

The authors would like to thank N. Banerjee for fruitful discussions and M. Smithers for the scanning electron microscopy measurements. Financial support from the Chemical Sciences division of the Netherlands Organization for Scientific Research (NWO-CW) in the framework of the TOP and ECHO programmes is gratefully acknowledged. The development of the Sagnac microscope is supported by NSF grant (ECCS-1346603) and Sloan Research Fellowship (BR2013–116).

Received: April 11, 2014
Revised: July 18, 2014
Published online: August 28, 2014

[1] a) A. Ohtomo, D. A. Muller, J. L. Grazul, H. Y. Hwang, *Nature* **2002**, *419*, 378; b) A. Ohtomo, H. Y. Hwang, *Nature* **2004**, *427*, 423; c) D. A. Muller, N. Nakagawa, A. Ohtomo, J. L. Grazul, H. Y. Hwang, *Nature* **2004**, *430*, 657; d) H. N. Lee, H. M. Christen, M. F. Chisholm, C. M. Rouleau, D. H. Lowndes, *Nature* **2005**, *433*, 395.

[2] a) A. Stanishevsky, S. Aggarwal, A. S. Prakash, J. Melngailis, R. Ramesh, *J. Vac. Sci. Technol., B* **1998**, *16*, 3899; b) C. S. Ganpule, A. Stanishevsky, Q. Su, S. Aggarwal, J. Melngailis, E. Williams, R. Ramesh, *Appl. Phys. Lett.* **1999**, *75*, 409.

[3] a) A. Stanishevsky, B. Nagaraj, J. Melngailis, R. Ramesh, L. Khriachtchev, E. McDaniel, *J. Appl. Phys.* **2002**, *92*, 3275; b) H. Han, Y. Kim, M. Alexe, D. Hesse, W. Lee, *Adv. Mater.* **2011**, *23*, 4599.

[4] a) P. M. te Riele, G. Rijnders, D. H. A. Blank, *Appl. Phys. Lett.* **2008**, *93*, 233109; b) C.-V. Cojocaru, R. Nechache, C. Harnagea, A. Pignolet, F. Rosei, *Appl. Surf. Sci.* **2010**, *256*, 4777; c) I. Vrejoiu, A. Morelli, F. Johann, D. Biggemann, *Appl. Phys. Lett.* **2011**, *99*, 082906.

[5] a) W. Lee, H. Han, A. Lotnyk, M. A. Schubert, S. Senz, M. Alexe, D. Hesse, S. Baik, U. Gösele, *Nat. Nanotechnol.* **2008**, *3*, 402; b) X. Gao, L. Liu, B. Birajdar, M. Ziese, W. Lee, M. Alexe, D. Hesse, *Adv. Funct. Mater.* **2009**, *19*, 3450; c) X. Lu, Y. Kim, S. Goetze, X. Li, S. Dong, P. Werner, M. Alexe, D. Hesse, *Nano Lett.* **2011**, *11*, 3202.

[6] a) N. Banerjee, M. Huijben, G. Koster, G. Rijnders, *Appl. Phys. Lett.* **2012**, *100*, 041601; b) J. Karthik, A. R. Damodaran, L. W. Martin, *Adv. Mater.* **2012**, *24*, 1610; c) N. Banerjee, G. Koster, G. Rijnders, *Appl. Phys. Lett.* **2013**, *102*, 142909.
[7] a) A. Kumar, G. M. Whitesides, *Appl. Phys. Lett.* **1993**, *63*, 2002; b) Y. Xia, E. Kim, X.-M. Zhao, J. A. Rogers, M. Prentiss, G. M. Whitesides, *Science* **1996**, *273*, 347; c) X.-M. Zhao, Y. Xia, G. M. Whitesides, *Adv. Mater.* **1996**, *8*, 837.
[8] E. Kim, Y. Xia, G. M. Whitesides, *Nature* **1995**, *376*, 581.
[9] a) Y. Xia, G. M. Whitesides, *Angew. Chem., Int. Ed.* **1998**, *37*, 550; b) J. E. ten Elshof, S. U. Khan, O. F. Göbel, *J. Eur. Ceram. Soc.* **2010**, *30*, 1555.
[10] a) J. M. D. Coey, M. Viret, L. Ranno, K. Ounadjela, *Phys. Rev. Lett.* **1995**, *75*, 3910; b) C. B. Eom, R. J. Cava, R. M. Fleming, J. M. Phillips, R. B. Van Dover, J. H. Marshall, J. W. P. Hsu, J. J. Krajewski, W. F. Peck Jr, *Science* **1992**, *258*, 1766.
[11] a) W. Wu, K. H. Wong, C. L. Choy, Y. H. Zhang, *Appl. Phys. Lett.* **2000**, *77*, 3441; b) C. B. Eom, R. B. Van Dover, J. M. Phillips, D. J. Werder, J. H. Marshall, C. H. Chen, R. J. Cava, R. M. Fleming, D. K. Fork, *Appl. Phys. Lett.* **1993**, *63*, 2570.
[12] a) L. Pellegrino, M. Biasotti, E. Bellingeri, C. Bernini, A. S. Siri, D. Marré, *Adv. Mater.* **2009**, *21*, 2377; b) M. D. Nguyen, H. Nazeer, K. Karakaya, S. V. Pham, R. Steenwelle, M. Dekkers, L. Abelmann, D. H. A. Blank, G. Rijnders, *J. Micromech. Microeng.* **2010**, *20*, 085022.
[13] M. W. J. Prins, K.-O. Grosse-Holz, G. Müller, J. F. M. Cillessen, J. B. Giesbers, R. P. Weening, R. M. Wolf, *Appl. Phys. Lett.* **1996**, *68*, 3650.
[14] J. H. Park, E. Vescovo, H.-J. Kim, C. Kwon, R. Ramesh, T. Venkatesan, *Nature* **1998**, *392*, 794.
[15] M. Bowen, M. Bibes, A. Barthélémy, J.-P. Contour, A. Anane, Y. Lemaître, A. Fert, *Appl. Phys. Lett.* **2003**, *82*, 233.
[16] A. Urushibara, Y. Moritomo, T. Arima, A. Asamitsu, G. Kido, Y. Tokura, *Phys. Rev. B: Condens. Matter Mater. Phys.* **1995**, *51*, 14103.
[17] J. Z. Sun, W. J. Gallagher, P. R. Duncombe, L. Krusin-Elbaum, R. A. Altman, A. Gupta, Y. Lu, G. Q. Gong, G. Xiao, *Appl. Phys. Lett.* **1996**, *69*, 3266.
[18] G. Koster, B. L. Kropman, G. J. H. M. Rijnders, D. H. A. Blank, H. Rogalla, *Appl. Phys. Lett.* **1998**, *73*, 2920.
[19] J. A. Wigenius, M. Hamedi, O. Inganäs, *Adv. Funct. Mater.* **2008**, *18*, 2563.
[20] O. F. Göbel, M. Nedelcu, U. Steiner, *Adv. Funct. Mater.* **2007**, *17*, 1131.
[21] A. George, J. E. ten Elshof, *J. Mater. Chem.* **2012**, *22*, 9501.
[22] H. Boschker, M. Huijben, A. Vailionis, J. Verbeeck, S. Van Aert, M. Luysberg, S. Bals, G. Van Tendeloo, E. P. Houwman, G. Koster, D. H. A. Blank, G. Rijnders, *J. Phys. D: Appl. Phys.* **2011**, *44*, 205001.
[23] M. Huijben, L. W. Martin, Y.-H. Chu, M. B. Holcomb, P. Yu, G. Rijnders, D. H. A. Blank, R. Ramesh, *Phys. Rev. B: Condens. Matter Mater. Phys.* **2008**, *78*.
[24] M. Izumi, Y. Konishi, T. Nishihara, S. Hayashi, M. Shinohara, M. Kawasaki, Y. Tokura, *Appl. Phys. Lett.* **1998**, *73*, 2497.
[25] a) Z.-H. Wang, G. Cristiani, H.-U. Habermeier, *Appl. Phys. Lett.* **2003**, *82*, 3731; b) M. Mathews, F. M. Postma, J. C. Lodder, R. Jansen, G. Rijnders, D. H. A. Blank, *Appl. Phys. Lett.* **2005**, *87*, 242507.
[26] J. A. Osborn, *Phys. Rev.* **1945**, *67*, 351.
[27] C. R. Martin, I. A. Aksay, *J. Phys. Chem. B* **2003**, *107*, 4261.
[28] G. Rijnders, D. H. A. Blank, J. Choi, C.-B. Eom, *Appl. Phys. Lett.* **2004**, *84*, 505.
[29] R. Bachelet, F. Sánchez, J. Santiso, C. Munuera, C. Ocal, J. Fontcuberta, *Chem. Mater.* **2009**, *21*, 2494.
[30] J. Xia, P. T. Beyersdorf, M. M. Fejer, A. Kapitulnik, *Appl. Phys. Lett.* **2006**, *89*, 062508.
[31] Q. Gan, R. A. Rao, C. B. Eom, J. L. Garrett, M. Lee, *Appl. Phys. Lett.* **1998**, *72*, 978.
[32] a) R. F. Service, *Science* **1997**, *276*, 895; b) Y. C. Kong, D. P. Yu, B. Zhang, W. Fang, S. Q. Feng, *Appl. Phys. Lett.* **2001**, *78*, 407; c) M. H. Huang, S. Mao, H. Feick, H. Yan, Y. Wu, H. Kind, E. Weber, R. Russo, P. Yang, *Science* **2001**, *292*, 1897.
[33] a) M. Hiramatsu, K. Imaeda, N. Horio, M. Nawata, *J. Vac. Sci. Technol., A* **1998**, *16*, 669; b) J.-H. Lee, K.-H. Ko, B.-O. Park, *J. Cryst. Growth* **2003**, *247*, 119; c) Q. Wan, Q. H. Li, Y. J. Chen, T. H. Wang, X. L. He, J. P. Li, C. L. Lin, *Appl. Phys. Lett.* **2004**, *84*, 3654.